Hindawi
International Journal of Photoenergy
Volume 2022, Article ID 5700570, 16 pages
https://doi.org/10.1155/2022/5700570

Research Article

A Firefly Algorithm and Elite Ant System-Trained Elman Neural Network for MPPT Algorithm of PV Array

Yan Zhang,[1] Ya-jun Wang,[1] Han Li,[1,2] Jia-Bao Chang,[1] and Jia-qi Yu[1]

[1]*Department of Electronic and Information Engineering, Liaoning University of Technology, 121001, China*
[2]*Liaoning Wish Information Technology Co., Ltd, Jinzhou 121001, China*

Correspondence should be addressed to Ya-jun Wang; dxxywyj@lnut.edu.cn

Received 13 May 2022; Revised 8 October 2022; Accepted 18 October 2022; Published 8 November 2022

Academic Editor: Daniel T. Cotfas

This article proposes a novel MPPT algorithm based on the firefly algorithm and elite ant system-trained Elman neural network (FA-EAS-ElmanNN). First, the position of fireflies is randomly initialized by the firefly algorithm (FA), meanwhile the firefly individuals with higher attractiveness degree value are selected as the optimal solution. Second, the extra pheromones are artificially released to boost the positive feedback effect and convergence rate of the elite ant system (EAS). Third, the weight and threshold of the Elman neural network (ElmanNN) are updated by the FA and EAS. Also, the trained ElamnNN is employed to acquire the maximum voltage of the photovoltaic (PV) array. At last, the PID controller and PWM technology are adapted to regulate the switch time of the boost converter. Furthermore, MATLAB/Simulink is adopted to acquire the datasets of irradiance, temperature, and maximum voltage and validate the reliability and superiority of the proposed algorithm under complex atmospheric conditions. The tracking characteristic, response speed, and efficiency of the proposed MPPT algorithm are contrasted with the particle swarm optimization (PSO), ant colony optimization (ACO), ACO-artificial neural network (ACO-ANN), and PSO-RBF neural network (PSO-RBNFNN) algorithm via simulation. The efficiency of the FA-EAS-ElmanNN algorithm is 99.73%, compared with the ACO-ANN, PSO-RBFNN, PSO, and ACO algorithm, which is increased by 0.49%, 0.58%, 1.2% %, and 1.5%, respectively. Additionally, the experimental setup is built to demonstrate the tracking characteristic of the proposed MPPT algorithm.

1. Introduction

With the rapid consumption of conventional reserved fossil fuel, the energy crisis and environmental degradation have sparked great attention of humankind [1]. PV power generation has become one of the most promising technology, which has the advantages of nonpollution, omnipresent, and cost effective [2]. However, the irradiance level (G) and ambient temperature (T) exhibits remarkable impact on the power generation efficiency of the PV array [3]. In order to collect the maximum efficiency from the PV array, the MPP of the PV array is tracked by the MPPT algorithm [4]. Therefore, the innovation of the MPPT algorithms has become a hot research area in the PV systems.

Currently, numerous researches have been addressed to extract from higher efficiency of PV array using different MPPT algorithms. Conventional MPPT algorithms, such as the look-up table method, perturbation and observation (P&O) algorithm, and incremental conductance (INC) algorithm [5]. In spite of the excellent tracking characteristic of mentioned above methods, the tracking characteristic and stabilization accuracy cannot be balanced. On this basis, researchers proposed the improved conventional MPPT algorithm to improve the power waveform quality and robustness. The improved MPPT conventional algorithms, such as adaptive P&O (AP&O) method, PSO-AP&O method, and variable step size INC method. The improved conventional MPPT algorithm has slower convergence rate and higher oscillation compared with the intelligent algorithm.

A review paper [6] has demonstrated that the MPPT methods can be divided into the hardware and soft computing MPPT methods. Hardware methods mainly include electronic compensation and reconstruction. The electronic compensation method can improve the quality of electric

energy through the auxiliary circuit. However, the auxiliary circuit tends to increase the computational complexity of the PV systems and introduces high-order harmonics. Therefore, the hardware method is not equipped with universality [7].

At present, the major challenge in the PV system is posed by the nonlinearity and complexity of the implicit PV array. Hence, the soft computing MPPT method is employed to solve the nonlinear current-voltage (I-V) equation. Soft computing MPPT methods, such as PSO algorithm, artificial neural network (ANN), genetic algorithm (GA), butterfly algorithm (BA), fuzzy logical control (FLC), and slide model control (SMC) [8]. These soft computing MPPT algorithms can accurately track the MPP of PV systems. However, the convergence rate of the single intelligence algorithm is slow and the population is prone to prematurity [9]. Therefore, the hybrid metaheuristic algorithms are proposed to enhance the tracking characteristic and respond speed of single MPPT algorithms. The hybrid metaheuristic algorithms, such as PSO-GA, GA-FLC, PSO-FA, and model prediction-Kalman filtering algorithm (MP-KFA) [10]. These recent hybrid metaheuristic algorithms have better tracking characteristic and higher efficiency than the single one.

In this context, many hybrid metaheuristic algorithms have developed in literature to improve the tracking characteristic of MPPT algorithms. In [11], Shams et al. developed an improved BA to differentiate the different partial shading patterns and solar intensity. The authors of [12] presented a new MPPT algorithm based on the improved squirrel search algorithm (ISSA). The ISSA has stronger tracking characteristic and higher efficiency than the conventional SAA. In [13], an improved differential evolution (DE) algorithm has introduced for tracking the global MPP (GMPP). In [14], Li et al. introduced an overall distribution PSO MPPT algorithm to improve the convergence rate and population diversity of the traditional PSO algorithm. The authors of [15] considered a novel leaky least mean logarithmic fourth (LLMLF) control strategy to improve the power quality and provide reactive power compensation for PV system. In [16], Kumar et al. developed a novel leaky least logarithmic absolute difference based on INC MPPT algorithm to mitigate the inherent problems of conventional INC algorithm such as tracking characteristic and stabilization accuracy issues. The authors of [17] introduced an improved optimal control strategy based on KFA to maximize power extraction from PV array. In [18], Kumar et al. proposed a self-tuned P&O algorithm to enhance the respond speed and steady-state oscillation of conventional P&O algorithm.

This article proposes a novel MPPT algorithm based on the firefly algorithm and elite ant system-trained Elman neural network (FA-EAS-ElmanNN). The FA and EAS are adopted to acquire the weight and threshold of the ElmanNN, and the maximum voltage (V_{mp}) of the PV array is predicted by the trained ElmanNN. In addition, the PID controller and PWM technology are applied to regulate the switch time of the MOSFET. Specifically, the major contributions are as follows: (1) the tracking characteristics, efficiency, and response speed of the MPPT algorithm are improved by the FA-EAS-ElmanNN algorithm; (2) the reliability and superiority of the proposed MPPT algorithm have been validated by MATLAB/Simulink. Additionally, the FA-EAS-ElmanNN algorithm is contrasted with the ACO-ANN, PSO-RBFNN, PSO, and ACO algorithms under five variable atmospheric conditions; (3) an experimental setup is built to demonstrate the tracking characteristic of the FA-EAS-ElmanNN algorithm.

The structure is concluded as follows: Section 2 describes the model of the PV array and boost converter; Section 3 introduces the ElmanNN, FA, and EAS and proposed MPPT algorithm; Sections 4 and 5 describe the simulation and experimental results, respectively; Section 6 describes the conclusion.

2. The Operational Principle of Photovoltaic Power System

PV power generation system consists of the PV array, PWM, DC-DC converter, MPPT controller, and load [19]. Figure 1 illustrates the framework of PV system with MPPT algorithm.

As shown in Figure 1, the acquired voltage and current is fed into the MPPT algorithm to obtain the modulated quantity. In addition, the modulated quantity is compared with the high-frequency carrier signal to adjust the switch time of the switch tube. Actually, the internal resistance matches with the load impedance by adjusting the PV array working voltage to ensure that the PV system always nearby the MPP.

2.1. Model of PV Array. The single diode model (SDM) has dark currents and compound losses under lower irradiance level. Therefore, the dual diode model (DDM) is selected to thoroughly characterize the output characteristics of PV array in this study. The PV array DDM model is introduced in Figure 2.

The output current formula of the PV array DDM model is introduced in

$$I = nI_{ph} - nI_{D1}\left[\exp\left(\frac{U/m + R_s I/n}{A_1 V_T}\right) - 1\right] - nI_{D2}\left[\exp\left(\frac{U/m + R_s I/n}{A_2 V_T}\right) - 1\right] - \frac{nU + mIR_s}{mR_{sh}}, \tag{1}$$

where R_s is the series resistance, R_{sh} is the shunt resistance, I is the output current of PV array, U is the output voltage of PV array, I_{ph} is the photoelectric current, I_o is the saturation current, I_{D1} and I_{D2} are the diode dark current, A_1 and A_2 are the ideal parameters for diode, $V_T = KT/q$, K is Boltzmann constant ($K = 1.38 \times 10^{-23}$ J/K), q is Coulomb constant ($q = 1.6 \times 10^{-19}$ C), T is the ambient temperature, and m and n are the series and parallel number of PV array, respectively [20].

Equation (1) is a transcendental equation, which is difficult to solve, and the PV array cannot always work nearby the MPP under standard test conditions (STC, $G_{ref} = 1000$ W/m^2, $T_{ref} = 25$°C). Therefore, it is essential to modify the correlation coefficient of PV array. Equations (2)–(7) are the modified equations of the PV array [21].

$$\Delta G = \frac{G}{G_{ref}} - 1, \tag{2}$$

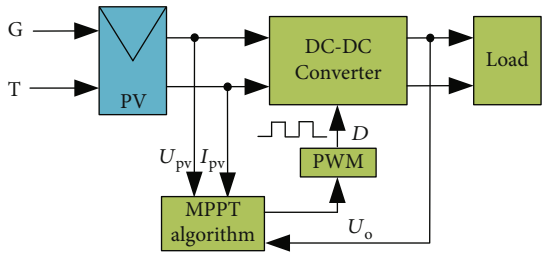

Figure 1: Framework of PV system with MPPT.

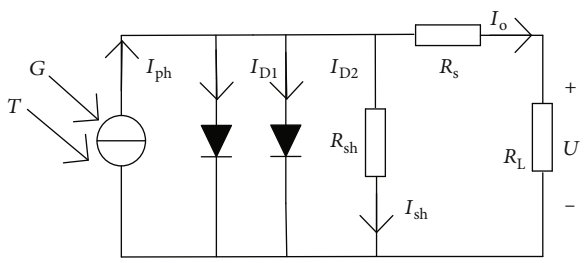

Figure 2: PV array DDM model.

$$\Delta T = T - T_{\text{ref}}, \tag{3}$$

$$I_{\text{scc}} = I_{\text{sc}}(1 + a\Delta T)\frac{G}{G_{\text{ref}}}, \tag{4}$$

$$V_{\text{occ}} = V_{\text{oc}}(1 - c\Delta T)\text{In}(e + b\Delta G), \tag{5}$$

$$I_{\text{mm}} = I_{\text{m}}(1 + a\Delta T)\frac{G}{G_{\text{ref}}}, \tag{6}$$

$$V_{\text{mm}} = V_{\text{m}}(1 - c\Delta T)\text{In}(e + b\Delta G), \tag{7}$$

where A, B, C, I_{scc}, V_{occ}, I_{mm}, and V_{mm} are the modified parameters. The specific parameters of the PV array under STC are as follows: open-circuit voltage $U_{\text{oc}} = 37.3$ V, short-circuit current $I_{\text{sc}} = 8.66$ A, MPP voltage $U_{\text{mp}} = 30.3$ V, MPP current $I_{\text{mp}} = 8.15$ A, MPP power $P_{\text{m}} = 250.205$ W, the temperature coefficient of the open-circuit voltage is -0.36091%/deg.c, and the temperature coefficient of the short-circuit current is 0.086998%/deg.c. Figure 3 illustrates the characteristic of PV array at changing G and T.

From Figure 3(a), the characteristics of PV array are the unimodal function with one MPP, and the MPP will drift with the irradiance and temperature [22]. In Figure 3(b), the voltage of PV array (U_{pv}) decreases and the current (I_{pv}) increases with the ambient temperature. Therefore, to maximize the efficiency of the PV array, the MPPT algorithm should be adopted to track the MPP of the PV array.

2.2. Modeling of Boost Converter. Currently, DC–DC converter includes boost converter, Cuk converter, forward converter, push-pull converter, and more. The boost converter has the characteristics of simple structure and driving [23]. The topology of the PV boost converter is given in Figure 4. The electrical boost converter parameters are as follows: filter capacitor $C = 100\,\mu$F, boost inductor $L = 2$ mH, output resistance $R = 20\,\Omega$, and output capacitor $C_1 = 100\,\mu$F. Moreover, C_1 and L are employed to eliminate the voltage ripple and high harmonic, respectively. According to the voltage-second balance principle, the inductor current is a fixed value, i.e., $I_{\text{pv}} = I_{\text{L}}$.

According to the Kirchhoff Voltage Law (KVL), the state formula of the PV boost converter is as follows:

$$\begin{cases} \dfrac{\text{d}I_{\text{pv}}}{\text{d}t} = \dfrac{U_{\text{pv}} - U_{\text{o}}}{L} + u\dfrac{U_{\text{o}}}{L}, \\ \dfrac{\text{d}U_{\text{o}}}{\text{d}t} = \left(-\dfrac{U_{\text{o}}}{RC_1} + \dfrac{I_{\text{pv}}}{C_1}\right) - u\dfrac{I_{\text{pv}}}{C_1}, \end{cases} \tag{8}$$

where I_{pv} and U_{pv} are the PV array current and voltage, respectively, U_{o} represents the output voltage of boost converter, R is output resistance, C_1 is the output capacitor, μ is the control variable $\in [0, 1]$, and the boost converter working voltage can be adjusted by controlling the on-off of the MOSFET.

3. System Structure and Proposed Algorithm

Since the ElmanNN has slow convergence rate and unstable learning rate, a novel MPPT algorithm based on the firefly algorithm and elite ant system-trained Elman neural network is proposed in this study. Figure 5 shows the schematic diagram of the FA-EAS-ElmanNN algorithm.

In Figure 5, V_{pv} and V_{ref} are the voltage and maximum reference voltage of the PV array, respectively, G is irradiance, and T is temperature. The specific steps of the proposed MPPT algorithm are as follows. First, the datasets of irradiance, temperature, and maximum voltage are acquired by MATLAB. The irradiance and temperature are the PV system inputs, and the output is the maximum voltage. Second, the weight and threshold of ElmanNN are acquired by the EAS and FA, and the maximum voltage of the PV array is predicted by the trained ElmanNN. Finally, PID controller and PWM technology are employed to adjust the switch time of the MOSFET Q.

3.1. Elman Neural Network. In 1990, ElmanNN was proposed based on the BP neural network (BPNN) by Jeffery L. ElmanNN is a typical dynamic recurrent neural network, which consists of the input layer, hidden layer, and connection layer (state layer) as well as output layer [24]. Figure 6 shows the basic structure of ElmanNN. The connection layer is a particular layer of ElmanNN, which is used to memorize the output of hidden layer at the previous moment and input the previous value prediction to the hidden layer after delay and storage. The ElmanNN is adopted to predict the maximum reference voltage (V_{ref}) according to G and T. In addition, the mean squared error (MSE) is selected as the cost function to evaluate the performance and precision of the ElmanNN, which is given in Equation (9). Figure 7 illustrates the maximum voltage of the PV array under changing G and T.

$$\text{MSE} = \frac{1}{n}\sum_{i=1}^{n}\sum_{j=1}^{m}\left[R_{\text{j}}(i) - N_{\text{j}}(i)\right]^2, \tag{9}$$

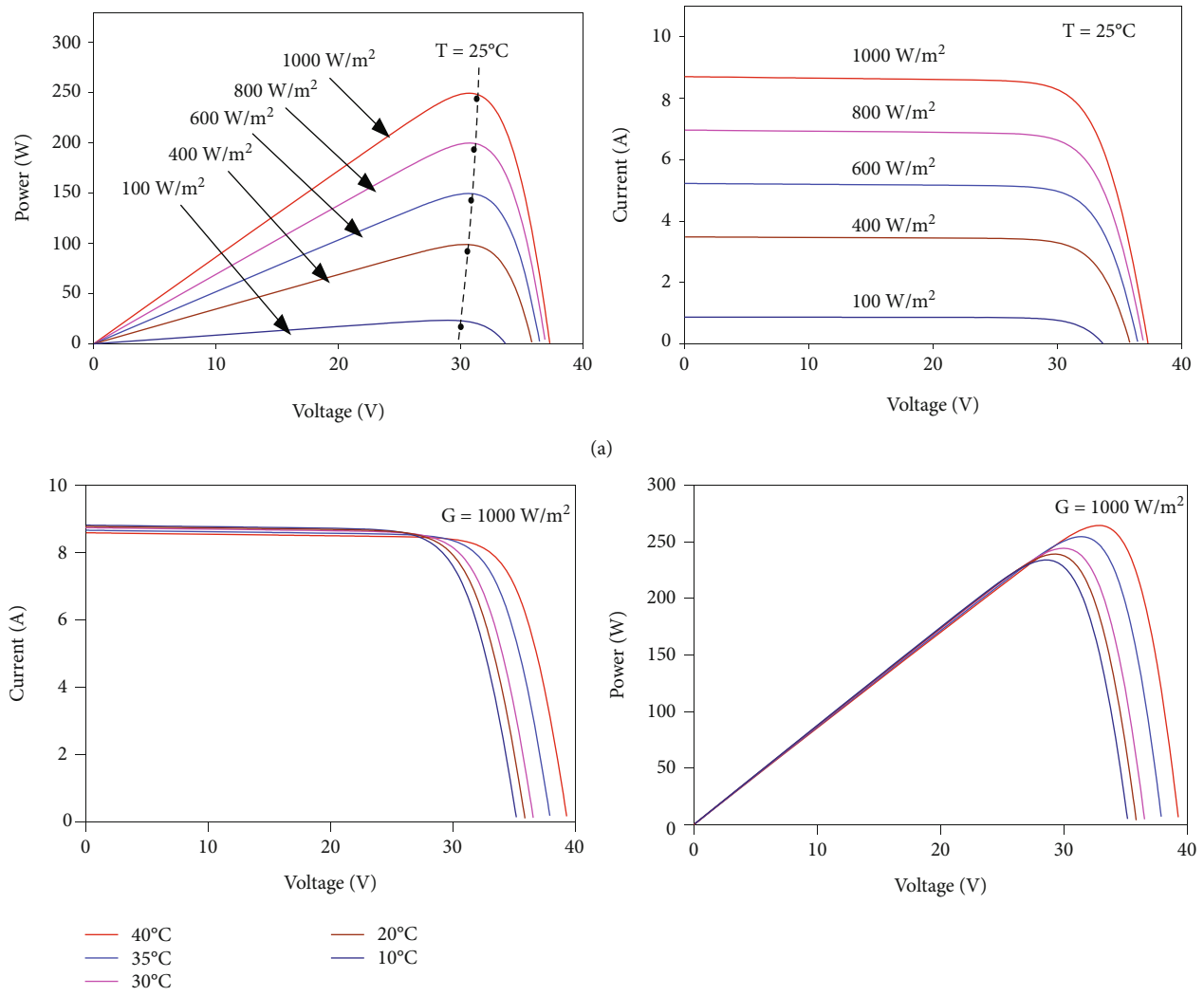

Figure 3: Characteristic of PV array at (a) changing G and (b) changing T.

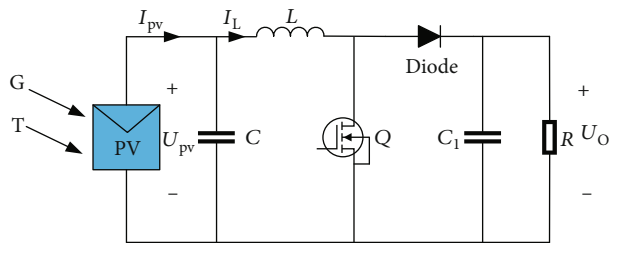

Figure 4: Topology of PV Boost converter.

where n represents the input datasets, m indicates the output datasets, and $R_j(i)$ and $N_j(i)$ are the true value and target value, respectively.

In this study, a general ElmanNN mathematical model is described as follows:

$$V_{ref} = f[G(k), T(k)], \tag{10}$$

where $G(k)$ represents the irradiance, $T(k)$ indicates the temperature, and V_{ref} is the MPP voltage of PV array.

3.2. Firefly Algorithm (FA). Podder et al. proposed the FA based on the characteristic of the information exchange and mutual attraction between firefly individuals [25]. FA has a good convergence rate and reliability. The firefly individuals will move toward the brighter one to search the population optimal solution in the competition and cooperation processes. The brightness value of the fireflies determines the individual quality and evolution direction, and the attractiveness value of the fireflies determines the distance and speed between the firefly individuals and population optimal solution. In the search process, the light intensity and attractiveness value determine the performance of the FA.

The relative brightness and attractiveness of each firefly are expressed as follows [26]:

$$I = I_0 e^{-\gamma r_{ij}}, \tag{11}$$

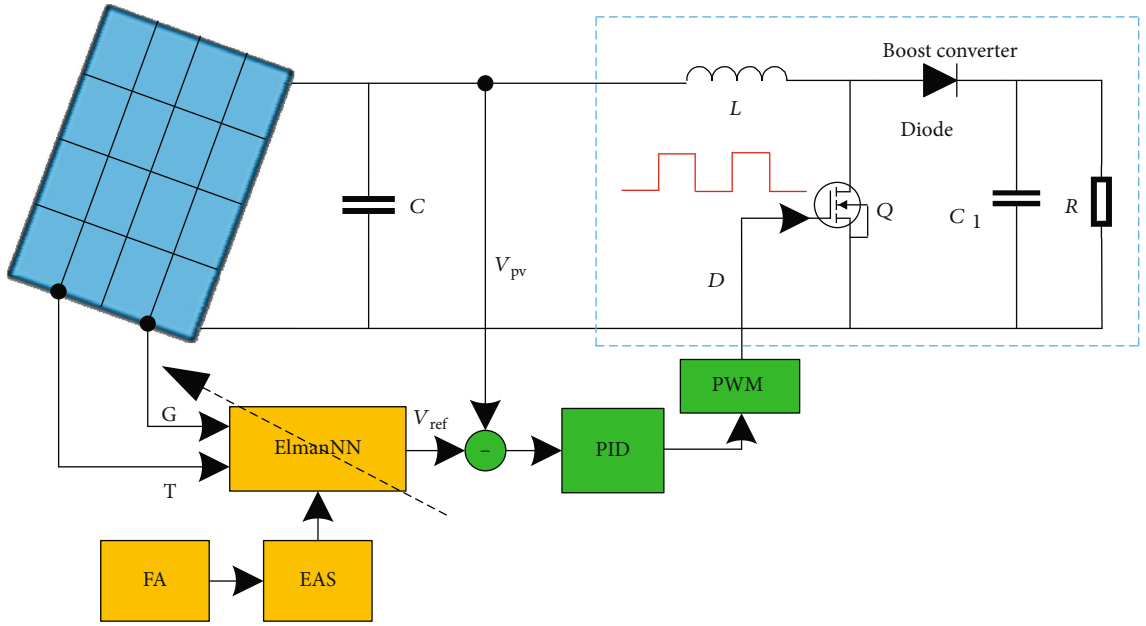

Figure 5: Schematic diagram of the FA-EAS-ElmanNN algorithm.

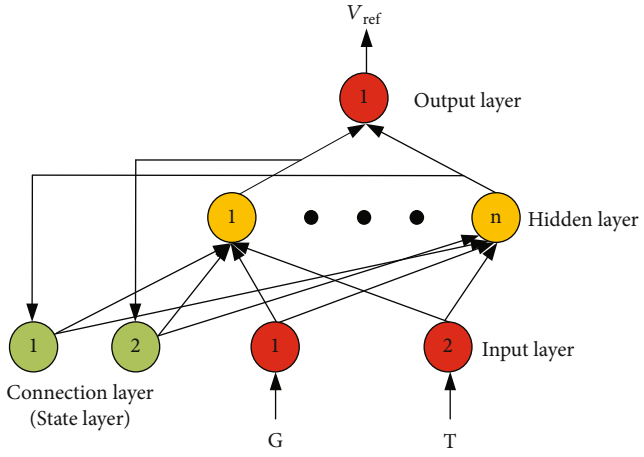

Figure 6: The structure of ElmanNN.

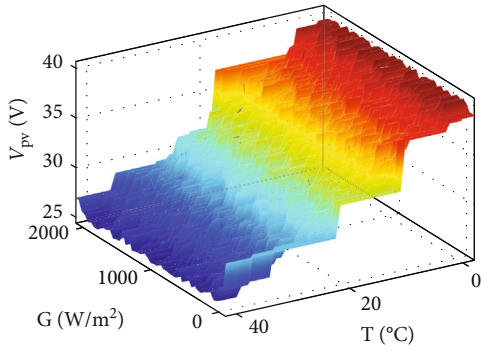

Figure 7: Maximum voltage of PV array at changing G and T.

$$\beta = \beta_0 e^{-\gamma r_{i,j}^2}, \tag{12}$$

where I_0 represents the maximum initial brightness of the fireflies, γ is the light absorption coefficient, β_0 is the maximum attraction, and r_{ij} is the Cartesian distance between two fireflies.

The position of population is updated by the

$$x_{i+1} = x_i + \beta\left(x_j - x_i\right) + \alpha\left(\text{rand} - \frac{1}{2}\right), \tag{13}$$

where x_i and x_j are the spatial positions of fireflies, α is the step factor, $\alpha \in [0, 1]$, and rand is the random number within [0, 1].

3.3. Elite Ant System (EAS). Dr. Gambardella developed the ant colony system (ACS) to improve the convergence rate of the conventional ACO algorithm [27, 28]. In fact, the ACO algorithm approaches the optimal individual through the competition and cooperation processes among the ant individuals. The distance of the ant colony is inversely proportional to the pheromone concentration. In the process of foraging, ants release a certain amount of pheromones, and the parent and offspring populations will gradually move toward the individual optimal solution under the positive feedback [29]. The convergence rate and prediction accuracy of the ACO algorithm depend on the state transition and the pheromone update model [30].

The pheromone update model of ACO algorithm mainly includes ant-cycle, ant-quantity, and ant-density models. The ant-cycle model is a global pheromone update strategy, and the pheromone of each ant is updated after the position information of the population is updated. Ant-quantity and ant-density models are the local update strategy, and the

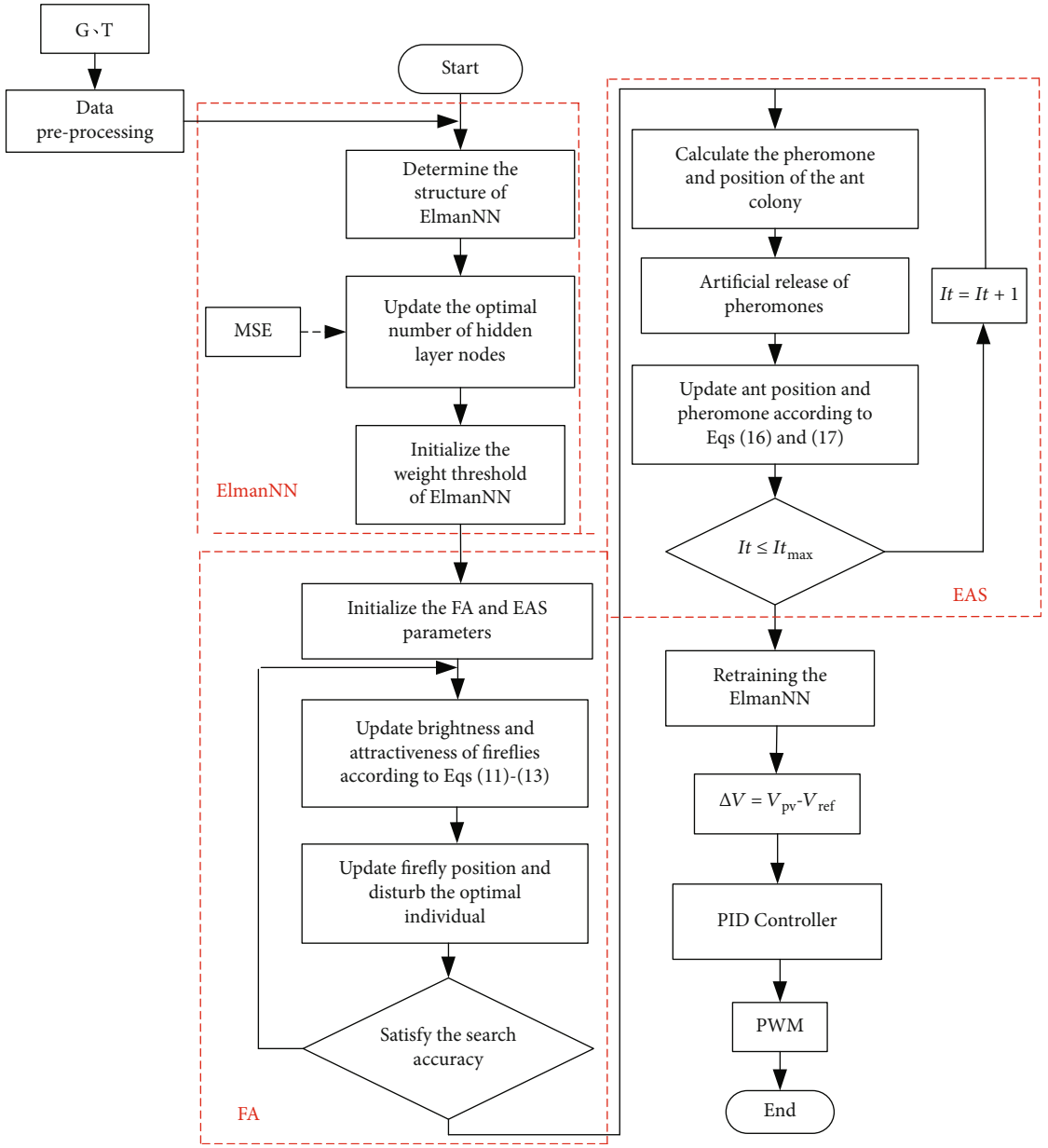

Figure 8: The flow chart of EAS-FA-ElmanNN.

pheromone concentrations of each ant are updated after each iteration. The pheromone concentration of the ant-quantity model is related to the initial parameter, while the pheromone concentration of the ant-density model is the fixed value. Equations (14) and (15) are the transfer probability and pheromone update equation of ACO algorithm.

$$P_{ij}^{k}(t) = \begin{cases} \dfrac{\left[\tau_{ij}(t)\right]^{a}\left[\eta_{ij}(t)\right]^{\beta}}{\sum_{s\in J_k(i)}\left[\tau_{ij}(t)\right]^{a}\left[\eta_{ij}(t)\right]^{\beta}}, & J \in J_k(i) \\ 0, & j \notin J_k(i) \end{cases}, \tag{14}$$

$$\begin{cases} \tau_{ij}(t+1) = (1-\rho)\tau_{ij}(t) + \Delta\tau_{ij}, \\ \Delta\tau_{ij} = \sum_{i=1}^{m}\left(\dfrac{Q}{L_k}\right), \end{cases} \tag{15}$$

where $P_{ij}^{k}(t)$ represents the selection probability of ants, α is the importance degree of pheromone, β is the relative importance of heuristic factor, η_{ij} is the heuristic factor, $\tau_{ij}(t)$ is the pheromone concentration, Q is the sum of pheromone concentration, ρ is the pheromone volatility, $\Delta\tau_{ij}$ is the sum of pheromone concentration increment, k is the ant number, and m is the number of the ant.

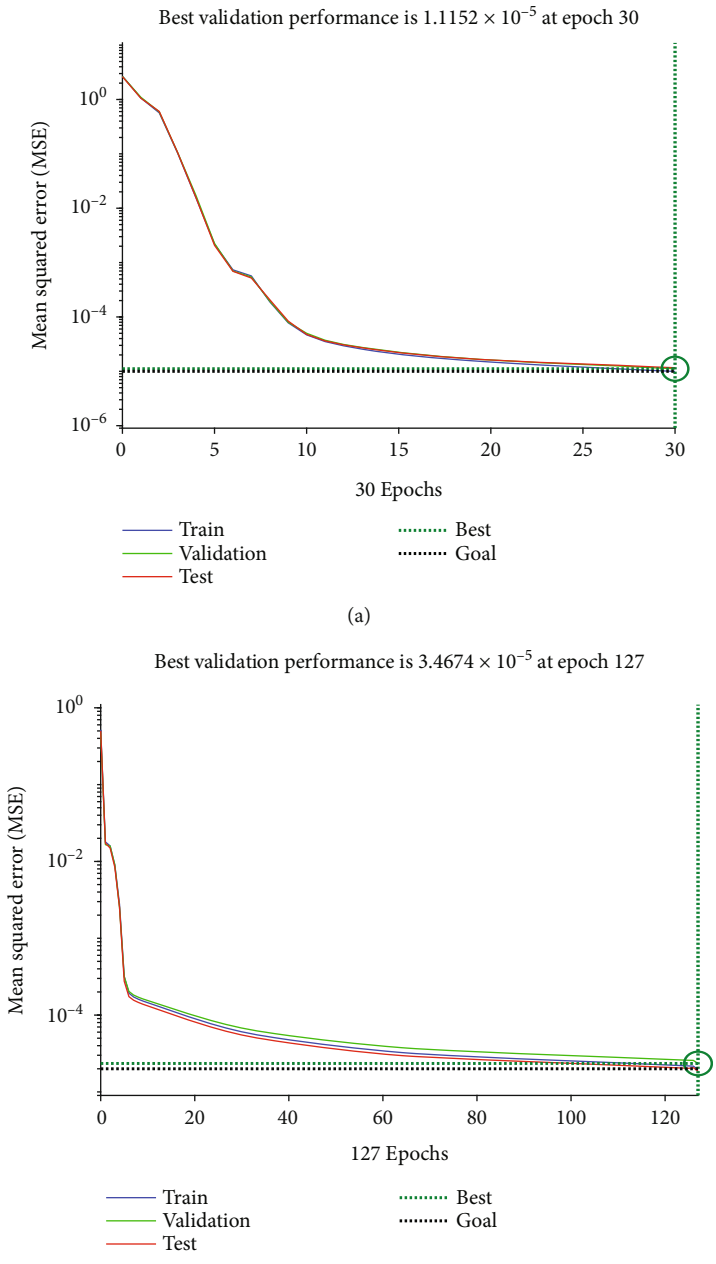

Figure 9: The best performance curves of (a) trained ElmanNN (b) conventional ElmanNN.

Since the ACO algorithm has slow convergence rate and long search time, an EAS control strategy is proposed in this paper. Moreover, the extra pheromones are artificially released to improve the positive feedback effect and convergence rate. The parent and offspring populations are ranked according to Equations (16) and (17), only the first w-1 ants can release pheromones in the search process. In addition, the fitness value (f) is employed to judge the population concentration and improve the convergence rate of the EAS according to the Equation (18). The pheromone update equations of the EAS are as follows:

$$\Delta\tau_{ij} = \sum_{k=1}^{w}(1-\rho)\Delta\tau_{ij}^{k} + e\Delta\tau_{ij}^{best}, \tag{16}$$

$$\Delta\tau_{ij}^{best} = \sum_{r=1}^{w-1}(w-r)\frac{Q(\mathrm{MSE}_{train} + \mathrm{MSE}_{test})}{Sl}, \tag{17}$$

$$\begin{cases} \rho_{i+1} = \rho_i, f_{i+1} \le f_{,i} \\ \rho_{i+1} = 0.95\rho_i, f_{i+1} > f_i, \end{cases} \tag{18}$$

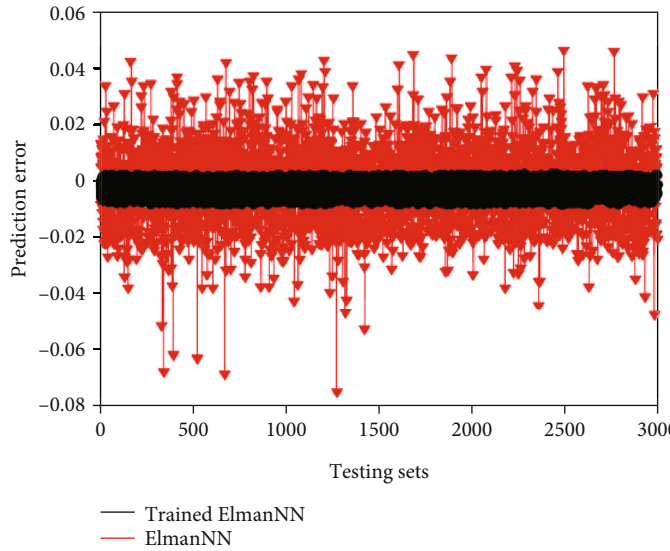

Figure 10: The prediction error of conventional and trained ElmanNN.

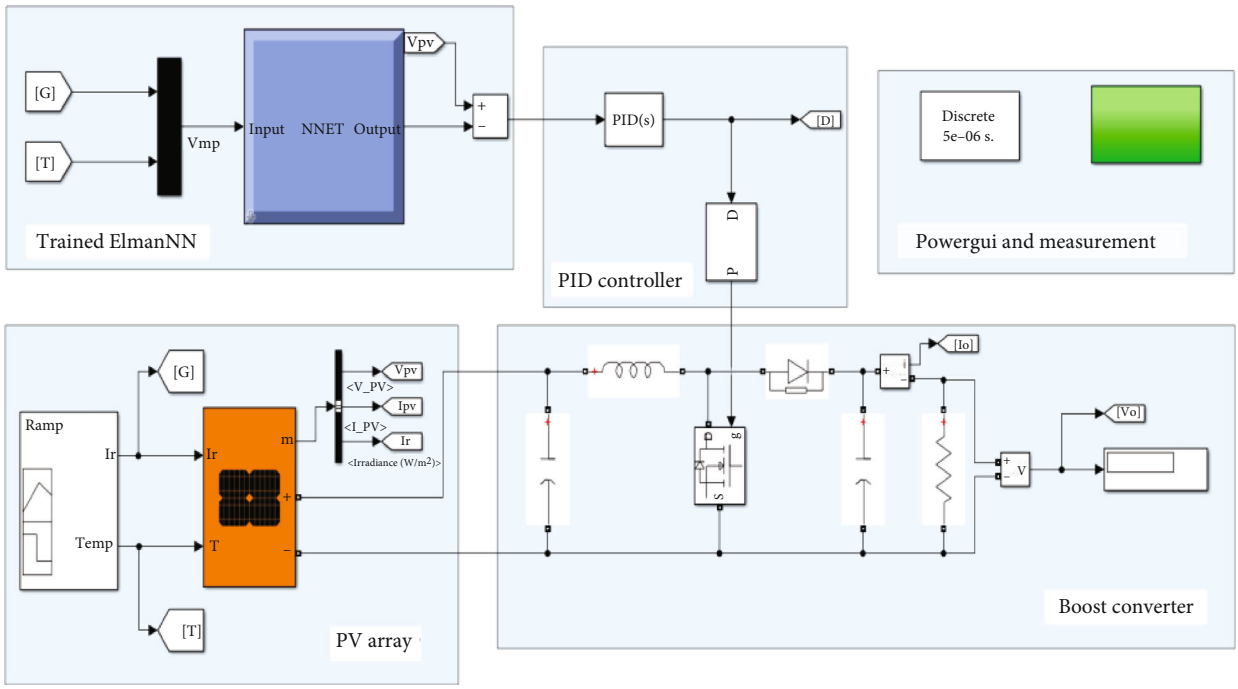

Figure 11: Simulation model of FA-EAS-ElmanNN control based MPPT.

where e is the weight adjustment coefficient, ρ is pheromone volatility, w is the number of ants, Q is the total amount of pheromone released by the first w -1 ants, and f is the loss function.

3.4. Datasets and Proposed MPPT Algorithm (FA-EAS-ElmanNN). Equations (19)–(21) are employed to acquire the datasets of irradiance, temperature, and maximum voltage (V_{mpp}). 70% of the datasets is selected as the training sets, and the rest is the testing sets. The inputs are the G and T, and the output is the maximum voltage.

$$G = (G_{max} - G_{min})\ \text{rand} + G_{min}, \tag{19}$$

$$T = (T_{max} - T_{min})\ \text{rand} + T_{min}, \tag{20}$$

$$V_{mpp} = V_{mps} + (\text{beta}(T - T_{ref})), \tag{21}$$

where $G_{max} = 1000\ \text{W/m}^2$, $G_{min} = 0\ \text{W/m}^2$, $T_{max} = 40^\circ\text{C}$, $T_{min} = 10^\circ\text{C}$, rand is the random number within [0, 1], V_{mps} is the maximum voltage of PV array under STC ($G_{ref} = 1000\ \text{W/m}^2$, $T_{ref} = 25^\circ\text{C}$), and beta is the temperature coefficient (beta = 0.36901). The flow chart of FA-EAS-ElamnNN algorithm is given in Figure 8. The specific steps of the proposed MPPT algorithm are as follows:

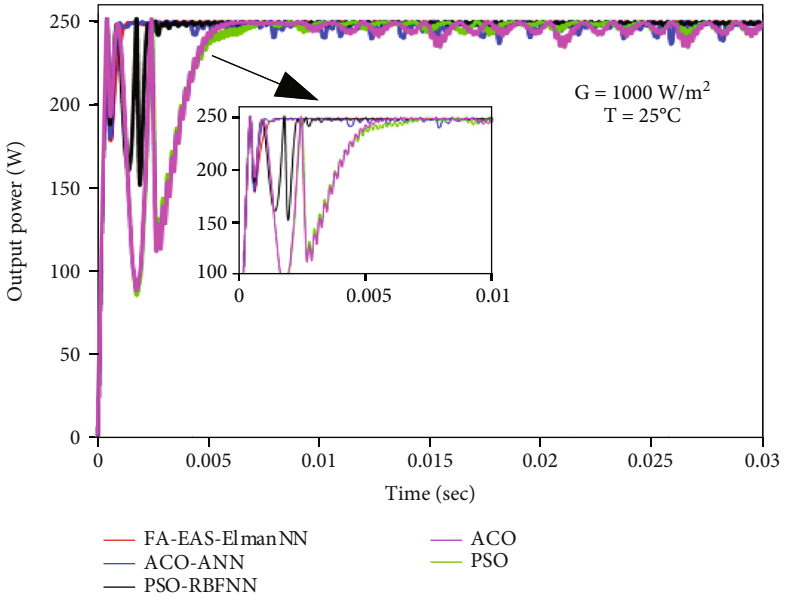

Figure 12: MPPT curve at startup.

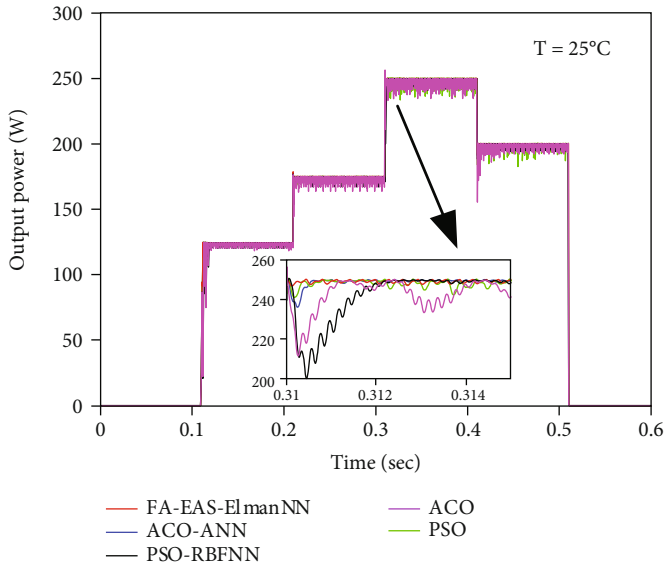

Figure 13: Output power of PV array under rapidly changing G ($T = 25^{\circ}C$).

(1) Equations (19)–(21) are employed to acquire the datasets of irradiance, temperature, and maximum voltage. Meanwhile, the MSE function is adopted to update the optimal number of hidden layer nodes of ElmanNN

(2) Initialize the FA and EAS parameters, such as Population size nPop, Cross-border coefficients U_b and L_b, Pheromone concenration tau, maximum attraction β_0, maximum initial brightness of the fireflies I_0, light absorption coefficient I, and maximum number of iteration It_{max}

(3) FA is used to calculate the relative brightness, attractiveness, and position of each firefly according to Equations (11)–(13). Furthermore, the position and attractiveness value of the brightest firefly is recorded, and the offspring populations are ranked in descending order. If the search accuracy is satisfied, perform the EAS algorithm; otherwise, return to step (3) to perform the FA

(4) According to Equations (16)–(18), the EAS is adopted to improve the positive feedback effect of

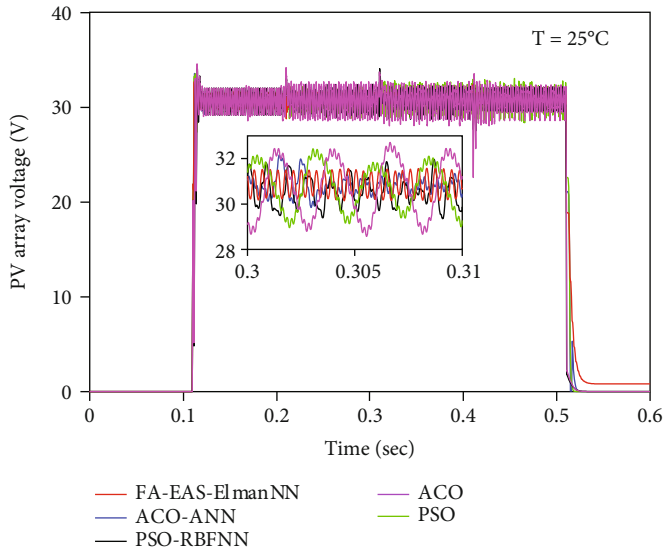

Figure 14: Voltage waveform of PV array under rapidly changing G.

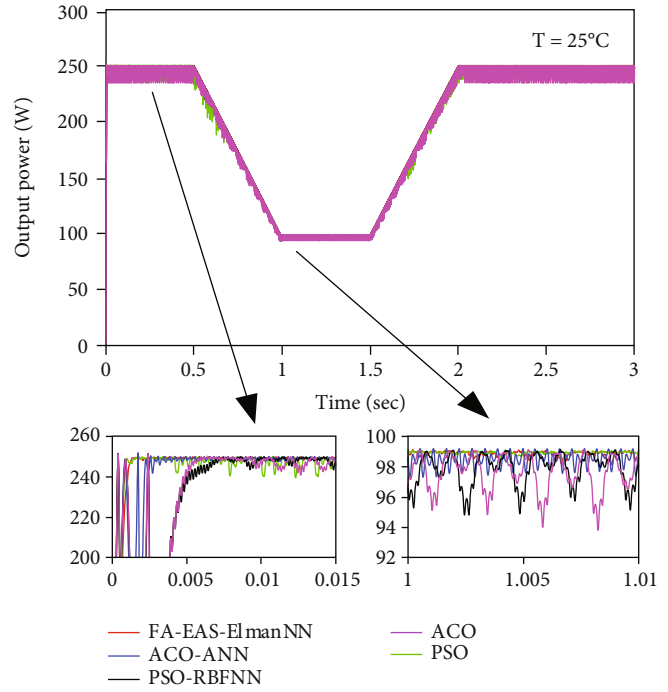

Figure 15: Output power of PV array under slowly changing G ($T = 25°C$).

pheromones. At the same time, the EAS is employed to guide the search direction of the ant colonies and improve the convergence rate

(5) If the current iteration number It is less than the maximum number of iteration It_{max}, then $It = It + 1$; otherwise, return to step (4)

(6) The weight and threshold of ElmanNN are updated by the FA and EAS. Moreover, the maximum voltage of the PV array is predicted by the trained ElmanNN

(7) The $\Delta V = V_{pv} - V_{ref}$ is used as the input of the PID controller, and the PWM technology is acquired to regulate the switch time of boost converter. The best performance curves of conventional ElmanNN and trained ElmanNN are given in Figure 9

As shown in Figure 9(a), the MSE and Epochs of the trained ElmanNN are 1.1152×10^{-5} and 30. In Figure 9(b), the MSE and Epochs of the conventional ElmanNN are 3.4674×10^{-5} and 127, respectively. Simulation results indicate

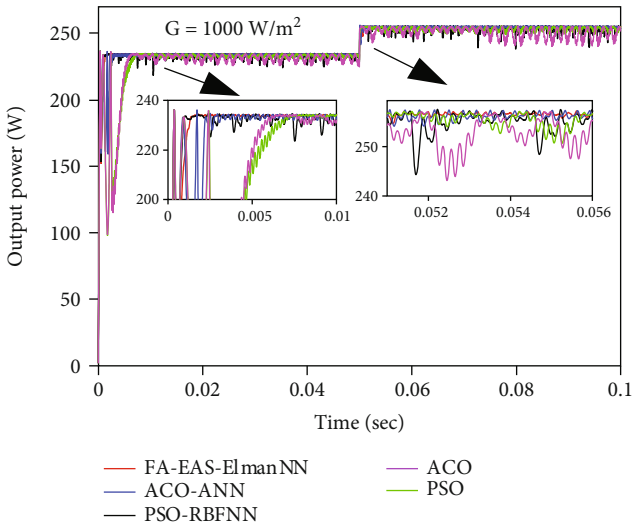

Figure 16: MPPT curve under rapidly changing T ($G = 1000\ \mathrm{W/m^2}$).

that the trained ElmanNN has better convergence rate and learning rate. Figure 10 illustrates the prediction error of the conventional and trained ElmanNN.

In Figure 10, the prediction error of the conventional ElmanNN is within [-0.08, 0.06]. The prediction error of the trained ElmanNN is within [-0.004, 0.004]. It should be mentioned that the prediction errors and convergence rate of ElmanNN has been improved in this study.

4. Simulation Results

The FA-EAS-ElmanNN algorithm is contrasted with the ACO-ANN [31], PSO-RBFNN [32], PSO, and ACO algorithms to validate the superiority of the proposed algorithm under five atmospheric conditions (STC, rapidly changing G , slowly changing G, suddenly changing T, and rapidly changing G and T). Furthermore, the tracking characteristics, stabilization accuracy, and efficiency of the five MPPT algorithms are analyzed.

4.1. Simulation Mode. The simulation model of FA-EAS-ElmanNN control based MPPT is given in Figure 11, which is mainly composed of the PV array, trained ElmanNN, PID controller, PWM generator, and boost converter.

4.2. MPPT Tracking Characteristic at Startup. Figure 12 shows the tracking characteristic of MPPT curve at startup under STC. The average output maximum power of five MPPT algorithm is about 250.08 W. Additionally, these MPPT algorithms can accurately track the MPP of the PV array, and the deviation from the nominal value of the PV array power is small.

As shown in Figure 12, at startup, the tracking time of the ACO-ANN, PSO-RBFNN, PSO, and ACO algorithms is 0.0024 s, 0.0031 s, 0.0061 s, and 0.0064 s, respectively. In addition, the tracking time of the FA-EAS-ElmanNN algorithm is 0.0011 s under the same condition. It can be seen clearly that the FA-EAS-ElmanNN algorithm has excellent tracking characteristic and stabilization accuracy, and the power chattering is lower.

4.3. MPPT Tracking Characteristics under Rapidly Changing G ($T = 25^{\circ}C$). Commonly, irradiance changes more frequently, and the efficiency of the PV array is highly influenced by the irradiance. Therefore, the proposed MPPT algorithm is applied and tested under rapidly changing G and slowly changing G. The parameters of rapidly changing G model are as follows: 0 s-0.1 s, $G = 0\ \mathrm{W/m^2}$; 0.101 s-0.2 s, $G = 500\ \mathrm{W/m^2}$; 0.201 s-0.3 s, $G = 700\ \mathrm{W/m^2}$; 0.301 s-0.4 s, $G = 1000\ \mathrm{W/m^2}$; 0.401 s-0.5 s, $G = 800\ \mathrm{W/m^2}$; 0.501 s-0.6 s, $G = 0\ \mathrm{W/m^2}$. Figure 13 illustrates the output power of the PV array under rapidly changing G ($T = 25^{\circ}\mathrm{C}$).

As shown in Figure 13, G beginning from $500\ \mathrm{W/m^2}$ increase to $700\ \mathrm{W/m^2}$ and afterward changes to $1000\ \mathrm{W/m^2}$; the tracking time of the FA-EAS-ElmanNN algorithm are 0.0011 s and 0.0013 s, respectively. As shown from Figure 13 that the tracking time of the ACO-ANN, PSO-RBFNN, PSO, and ACO algorithms is 0.0021 s, 0.0026 s, 0.0036 s, and 0.0041 s, respectively. Figure 14 shows the voltage waveform of the PV array under rapidly changing G.

In Figure 14, the steady state oscillation rate and MPP voltage of the FA-EAS-ElmanNN algorithm is 0.31% and 31.3 V, respectively. However, the steady state oscillation rate of the ACO-ANN, PSO-RBFNN, ACO, and PSO algorithms is 0.84%, 0.91%, 2.84%, and 3.14%. Moreover, the MPP voltage of the four compared MPPT algorithms is 30.3 V, 30.1 V, 29.57 V, and 29.35 V, respectively. Simulation result shows that the FA-EAS-ElmanNN algorithm has better tracking characteristic and robustness under rapidly changing G.

4.4. MPPT Tracking Characteristics under Slowly Changing G ($T = 25^{\circ}C$). In this study, a trapezoidal irradiance model is constructed according to the daily irradiance model of a block in the western China. The parameters of the slowly changing G model are as follows: 0 s~0.5 s, $G = 1000\ \mathrm{W/m^2}$; 0.5 s~1 s, G decreases from $1000\ \mathrm{W/m^2}$ to $400\ \mathrm{W/m^2}$; 1 s~1.5 s, $G = 400\ \mathrm{W/m^2}$; 1.5 s~2 s, G increases from $400\ \mathrm{W/m^2}$ to $1000\ \mathrm{W/m^2}$; 2 s~3 s, $G = 1000\ \mathrm{W/m^2}$. Figure 15 illustrates the output power of the PV array under slowly changing G.

From Figure 15, at startup, it is manifest that the tracking time of the FA-EAS-ElmanNN algorithm is 0.001 s, and the tracking time of the four compared algorithms are 0.0021 s, 0.0027 s, 0.0058 s, and 0.0064 s, respectively. The four compared algorithms show obvious power trailing phenomenon. Hence, the stabilization accuracy of the FA-EAS-ElmanNN algorithm is better than the four compared algorithms. It is quite clear that the FA-EAS-ElmanNN algorithm has excellent respond speed and lower oscillation amplitude under slowly changing G.

In summary, the FA-EAS-ElmanNN algorithm has better response speed and tracking characteristic, and the power waveform is smoother. Furthermore, the proposed MPPT algorithm has a lower waveform oscillation amplitude under changing G.

4.5. MPPT Tracking Characteristics under Rapidly Changing T ($G = 1000\ \mathrm{W/m^2}$). Rain and snow weather will cause the T

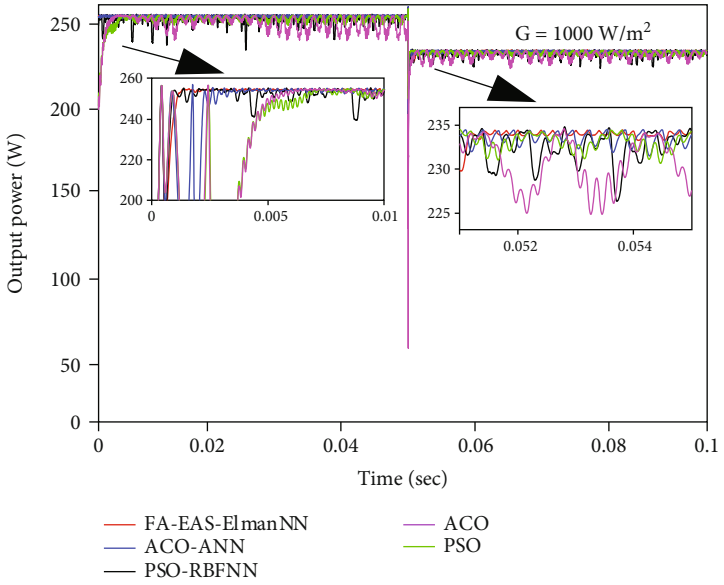

Figure 17: MPPT curve under rapidly decreasing T ($G = 1000\,\mathrm{W/m^2}$).

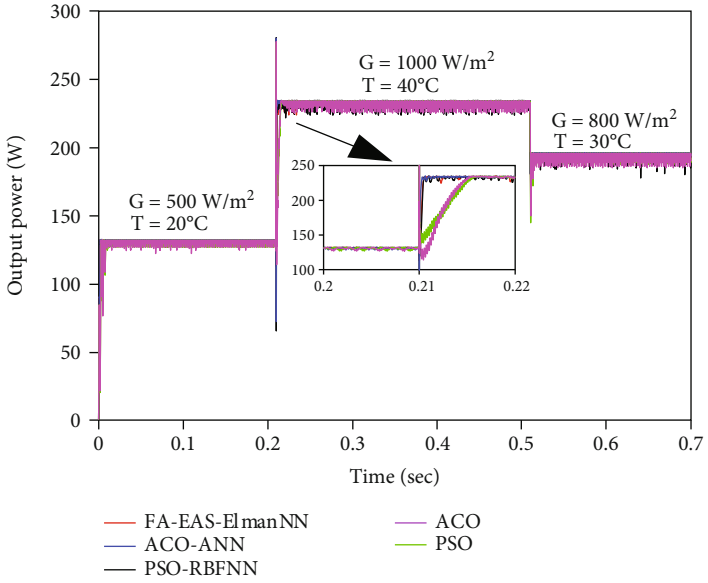

Figure 18: Output power of PV array under rapidly changing G and T.

changes, and the efficiency is highly influence by the ambient temperature. Figure 16 describes the simulation waveform of five MPPT algorithms under the condition that the T changes from 40°C to 20°C ($G = 1000\,\mathrm{W/m^2}$).

In Figure 16, at startup, the tracking time to the MPP of the FA-EAS-ElmanNN algorithm is 0.0013 s. However, the tracking time of the four compared algorithms is 0.0026 s, 0.0031 s, 0.0063 s, and 0.0074 s, respectively. The tracking time of the FA-EAS-ElmanNN algorithm is 0.0012 s when T decreases from 40°C to 20°C. However, the tracking time of the four compared algorithms is 0.0028 s, 0.0035 s, 0.007 s, and 0.009 s, respectively. The results clearly depict that the FA-EAS-ElmanNN algorithm exists better tracking characteristic. Figure 17 illustrates the simulation waveform of the five MPPT algorithms under the condition that T changes from 20°C to 40°C ($G = 1000\,\mathrm{W/m^2}$).

In Figure 17, T changes from 20°C to 40°C at 0.05 s; the FA-EAS-ElmanNN algorithm has better tracking characteristic, respond speed, and stabilization accuracy. It is manifested from the obtained results show that the FA-EAS-ElmanNN algorithm has better real-time performance and robustness than the four compared MPPT algorithms.

In summary, the proposed MPPT algorithm can efficiently track MPP of the PV array. Moreover, the FA-EAS-ElmanNN algorithm has a higher stabilization accuracy and tracking characteristic under rapidly changing T.

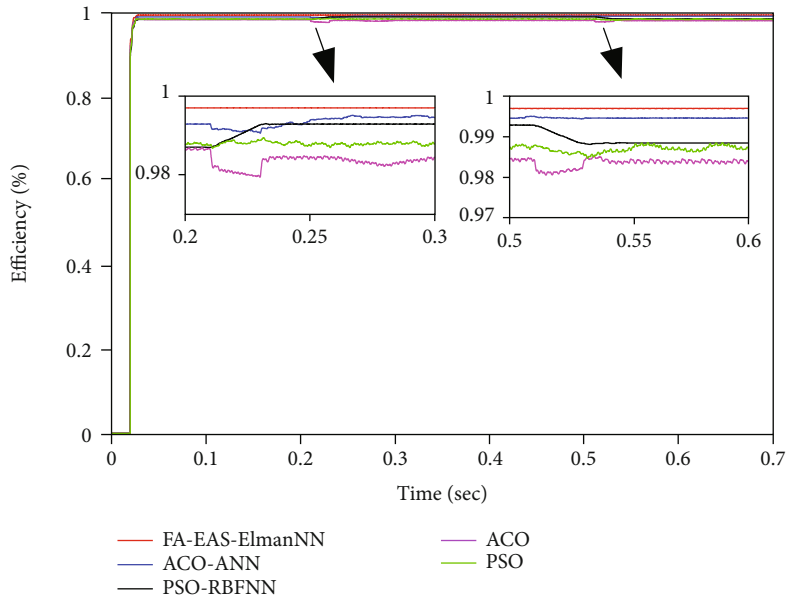

Figure 19: Efficiency under rapidly changing G and T.

Table 1: The results of five MPPT algorithms.

MPPT algorithm	Steady-state oscillation rate (%)			Power amplitude range (W)		
	0 s~0.2 s	0.2 s~0.5 s	0.5 s~0.7 s	0 s~0.2 s	0.2 s~0.5 s	0.5 s~0.7 s
FA-EAS-ElmanNN	0.31	0.35	0.33	134.6~136.3	238.9~240.7	193.4~195.6
ACO-ANN	0.84	0.89	0.86	131.1~135.6	233.3~239.4	187.3~194.7
PSO-RBFNN	0.91	0.94	0.92	130.5~135.3	232.1~239.3	186.3~194.8
PSO	2.84	2.85	2.84	126.4~137.3	223.5~241.4	181.3~195.5
ACO	3.14	3.17	3.15	116.8~137.6	217.9~241.1	180.2~195.7
MPPT algorithm	Efficiency (%)			Tracking time (s)		
	0 s~0.2 s	0.2 s~0.5 s	0.5 s~0.7 s	0 s~0.2 s	0.2 s~0.5 s	0.5 s~0.7 s
FA-EAS-ElmanNN	99.71	99.73	99.72	0.0011	0.0013	0.0011
ACO-ANN	99.13	99.24	99.19	0.0020	0.0022	0.0021
PSO-RBFNN	99.05	99.15	99.10	0.0027	0.0028	0.0027
PSO	98.39	98.53	98.44	0.0053	0.0056	0.0054
ACO	98.02	98.23	98.14	0.0057	0.0059	0.0057

4.6. MPPT Tracking Characteristics under Rapidly Changing G and T. PV array has severe nonlinear characteristic, and the photoelectric conversion efficiency is greatly influenced by the external environment. Therefore, the control quality of the five MPPT algorithms is analyzed under rapidly changing G and T. The parameters of G and T models are as follows: 0 s-0.2 s, $G = 500\ W/m^2$, $T = 20^\circ C$; 0.2 s-0.5 s, $G = 1000\ W/m^2$, $T = 40^\circ C$; 0.5 s-0.7 s, $G = 800\ W/m^2$, $T = 30^\circ C$. Figure 18 shows the simulation waveform of the five algorithms under rapidly changing G and T.

As shown in Figure 18, G beginning from $500\ W/m^2$ increases to $1000\ W/m^2$ and afterward decreases to $800\ W/m^2$; the tracking time of the FA-EAS-ElmanNN algorithm is 0.0011 s and 0.0013 s, respectively. Moreover, the tracking time of the ACO-ANN, PSO-RBFNN, ACO, and PSO algorithm is 0.0022 s, 0.0028 s, 0.0056 s, and 0.0059 s under the same condition. It should be noticed from results that the FA-EAS-ElmanNN algorithm has smaller power oscillation, and the tracking characteristic and adaptability are better than the four compared MPPT algorithms. Figure 19 illustrates the efficiency of the PV array under rapidly changing G and T.

As shown from Figure 19, the efficiency of the FA-EAS-ElmanNN algorithm is 99.73%. In contrast, the efficiency of the ACO-ANN, PSO-RBFNN, PSO, and ACO algorithm is 99.24%, 99.15%, 98.53%, and 98.23%, respectively. It can be observed that the FA-EAS-ElmanNN algorithm can acquire the maximum efficiency from the PV array, has better reliability and photoelectric conversion efficiency under rapidly G and T. The results of five MPPT algorithms are shown in Table 1.

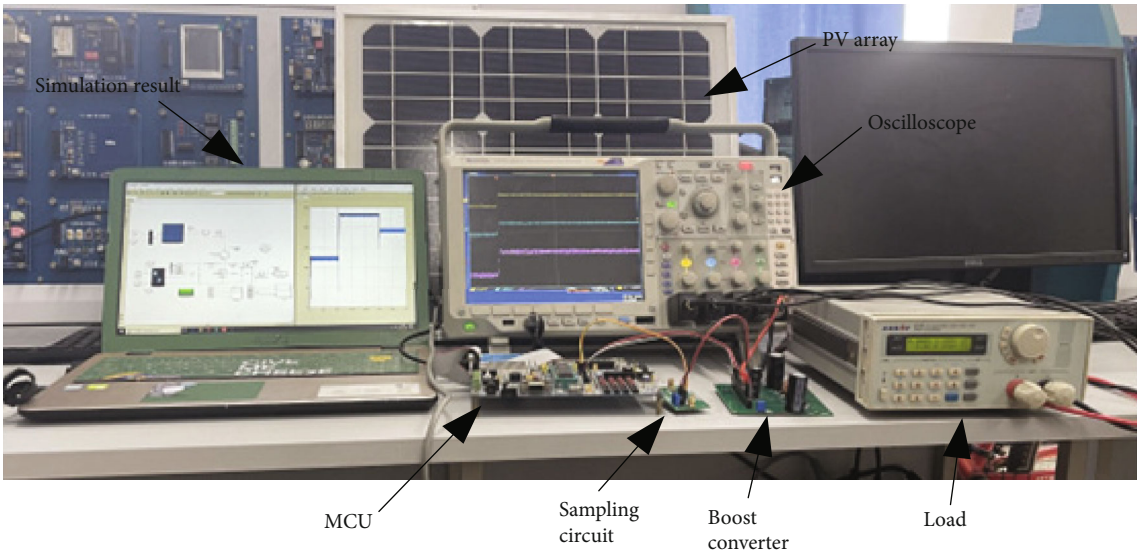

Figure 20: Experimental system with MPPT.

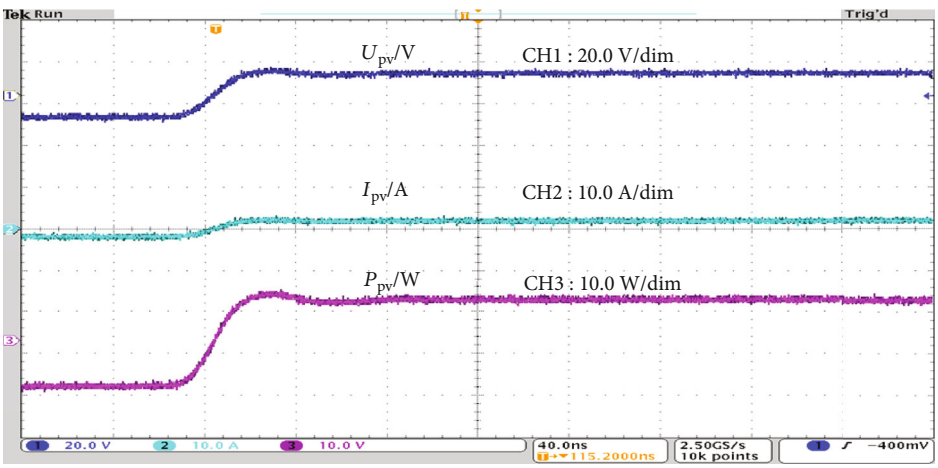

(a)

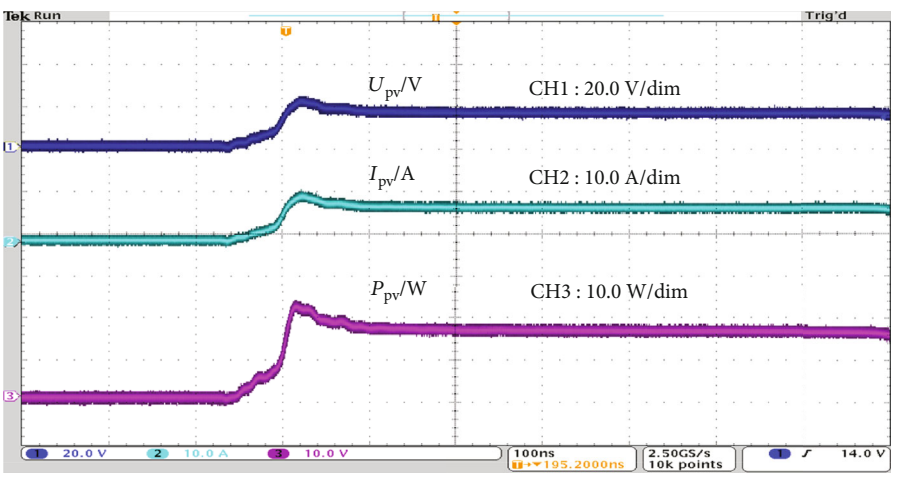

(b)

Figure 21: Tracking results under varying G (a) FA-EAS-ElmanNN algorithm and (b) PSO algorithm.

In conclusion, the obtained results indicate that the FA-EAS-ElmanNN algorithm can accurately track the MPP and has better tracking characteristic, efficiency, and anti-interference ability compared with the ACP-ANN, PSO-RBFNN, PSO, and ACO algorithm.

5. Experimental Setup and Results

The tracking characteristic of proposed algorithm is validated by the experimental system, which is shown in Figure 20. The experimental setup consists of the PV array, MCU, load, sampling circuit, oscilloscope, etc. Moreover, the FA-EAS-ElmanNN algorithm is contrasted with the PSO algorithm under varying G.

The main experimental steps of the FA-EAS-ElmanNN algorithm are as follows. First, the compiled program is downloaded to the controller by using the J-Link V8 simulator. Second, a group of lights is adopted to simulate the change of irradiance. Finally, the PV voltage, current, and power waveforms of the FA-EAS-ElmanNN and PSO algorithm are recorded, respectively. The tracking results under varying G for different MPPT algorithms are given in Figure 21.

As shown in Figure 21, the two MPPT algorithms can track the MPP of the PV array. It is evident that the tracking time to the MPP of the proposed algorithm is 13 ms. Furthermore, the tracking time the PSO algorithm is 21 ms. It can be observed from Figures 12–21 that the FA-EAS-ElmanNN algorithm has stronger tracking characteristic and stabilization accuracy.

6. Conclusion

Since the drawbacks of MPPT algorithm, such as weak respond speed and efficiency, a novel MPPT algorithm based on the firefly algorithm and elite ant system-trained Elman neural network is presented. The weight and threshold of the ElmanNN are updated by the FA and EAS. The obtained results indicated that the convergence rate and prediction accuracy of trained ElmanNN are optimized. Also, the tracking characteristic, stabilization accuracy, and power generation efficiency of MPPT algorithm are greatly improved. The most remarkable characteristic of the proposed MPPT algorithm is that only maximum voltage of the PV array is acquired by the irradiance level and ambient temperature, which makes the algorithm simple without other parameters. Through the analysis of simulation and experimental results, the conclusions are as follows:

(1) The proposed MPPT algorithm has good performance and universality under variable atmospheric conditions (STC, rapidly changing G, slowly changing G, suddenly changing T, and rapidly changing G and T)

(2) The comparison Table 1 states that the proposed MPPT algorithm is superiority to the ACO-ANN, PSO-RBFNN, PSO, and ACO algorithms in tracking characteristic, stabilization, and efficiency

(3) The future works will focus on the implementation of ANN on DC-DC converter practically

Data Availability

The irradiation and temperature datasets used to support the findings of this study are included within the article.

Conflicts of Interest

The authors declare that they have no conflict of interest.

Acknowledgments

This study was funded by the National Natural Science Foundation of China (grant: 61503169, 61802161), Natural Science Foundation of Liaoning Province (grant: 2020-MS-291), and Liaoning Province's Science and Technology Plan (Major) Project of "Exposing the Leader" (grant: 2022JH1/10400009).

References

[1] U. Yilmaz, O. Turksoy, and A. Teke, "Improved MPPT method to increase accuracy and speed in photovoltaic systems under variable atmospheric conditions," *International Journal of Electrical Power & Energy Systems*, vol. 113, pp. 634–651, 2019.

[2] S. Motahhir, A. El-Hammoumi, and A. El-Ghzizal, "Photovoltaic system with quantitative comparative between an improved MPPT and existing INC and P&O methods under fast varying of solar irradiation," *Energy Reports*, vol. 4, pp. 341–350, 2018.

[3] L. Shengqing, L. Fujun, Z. Jian, C. Wen, and Z. Donghui, "An improved MPPT control strategy based on incremental conductance method," *Soft Computing*, vol. 24, no. 8, pp. 6039–6046, 2020.

[4] Y. Mahmoud, M. Abdelwahed, and E. F. el-Saadany, "An enhanced MPPT method combining model-based and heuristic techniques," *IEEE Transactions on Sustainable Energy*, vol. 7, no. 2, pp. 576–585, 2015.

[5] S. Tang, Y. Sun, Y. Chen, Y. Zhao, Y. Yang, and W. Szeto, "An enhanced MPPT method combining fractional-order and fuzzy logic control," *IEEE Journal of Photovoltaic*, vol. 7, no. 2, pp. 640–650, 2017.

[6] J. Dadkhah and M. Niroomand, "Optimization methods of MPPT parameters for PV systems: review, classification, and comparison," *Journal of Modern Power Systems and Clean Energy*, vol. 9, no. 2, pp. 225–236, 2021.

[7] S. Messalti, A. Harrag, and A. Loukriz, "A new variable step size neural networks MPPT controller: review, simulation and hardware implementation," *Renewable & Sustainable Energy Reviews*, vol. 68, pp. 221–233, 2017.

[8] R. B. Bollipo, S. Mikkili, and P. K. Bonthagorla, "Critical review on PV MPPT techniques: classical, intelligent and optimisation," *IET Renewable Power Generation*, vol. 14, no. 9, pp. 1433–1452, 2020.

[9] B. Bendib, H. Belmili, and F. Krim, "A survey of the most used MPPT methods: conventional and advanced algorithms applied for photovoltaic systems," *Renewable & Sustainable Energy Reviews*, vol. 45, pp. 637–648, 2015.

[10] H. Rezk, A. Fathy, and A. Y. Abdelaziz, "A comparison of different global MPPT techniques based on meta-heuristic algorithms for photovoltaic system subjected to partial shading conditions," *Renewable & Sustainable Energy Reviews*, vol. 74, pp. 377–386, 2017.

[11] I. Shams, S. Mekhilef, and K. S. Tey, "Maximum power point tracking using modified butterfly optimization algorithm for partial shading, uniform shading, and and fast varying load conditions," *IEEE Transactions on Power Electronics*, vol. 36, no. 5, pp. 5569–5581, 2020.

[12] D. Fares, M. Fathi, I. Shams, and S. Mekhilef, "A novel global MPPT technique based on squirrel search algorithm for PV module under partial shading conditions," *Energy Conversion and Management*, vol. 230, pp. 113773–113785, 2021.

[13] K. S. Tey, S. Mekhilef, M. Seyedmahmoudian, B. Horan, A. T. Oo, and A. Stojcevski, "Improved differential evolution-based MPPT algorithm using SEPIC for PV systems under partial shading conditions and load variation," *IEEE Transactions on Industrial Informatics*, vol. 14, no. 10, pp. 4322–4333, 2018.

[14] H. Li, D. Yang, W. Su, J. Lü, and X. Yu, "An overall distribution particle swarm optimization MPPT algorithm for photovoltaic system under partial shading," *IEEE Transactions on Industrial Electronics*, vol. 66, no. 1, pp. 265–275, 2018.

[15] N. Kumar, B. Singh, and B. K. Panigrahi, "LLMLF-based control approach and LPO MPPT technique for improving performance of a multifunctional three-phase two-stage grid integrated PV system," *IEEE Transactions on Sustainable Energy*, vol. 11, no. 1, pp. 371–380, 2019.

[16] N. Kumar, B. Singh, B. K. Panigrahi, and L. Xu, "Leaky-least-logarithmic-absolute-difference-based control algorithm and learning-based InC MPPT technique for grid-integrated PV system," *IEEE Transactions on Industrial Electronics*, vol. 66, no. 11, pp. 9003–9012, 2019.

[17] N. Kumar, B. Singh, J. Wang, and B. K. Panigrahi, "A framework of L-HC and AM-MKF for accurate harmonic supportive control schemes," *IEEE Transactions on Circuits and Systems I: Regular Papers*, vol. 67, no. 12, pp. 5246–5256, 2020.

[18] N. Kumar, B. Singh, and B. K. Panigrahi, "Integration of solar PV with low-voltage weak grid system: using maximize-M Kalman filter and self-tuned P&O algorithm," *IEEE Transactions on Industrial Electronics*, vol. 66, no. 11, pp. 9013–9022, 2019.

[19] R. Celikel, M. Yilmaz, and A. Gundogdu, "A voltage scanning-based MPPT method for PV power systems under complex partial shading conditions," *Renewable Energy*, vol. 184, pp. 361–373, 2022.

[20] V. Balaji and A. P. Fathima, "Hybrid algorithm for MPPT tracking using a single current sensor for partially shaded PV systems," *Sustainable Energy Technologies and Assessments*, vol. 53, pp. 102415–102426, 2022.

[21] T. A. Boghdady, Y. E. Kotb, A. Aljumah, and M. M. Sayed, "Comparative study of optimal PV array configurations and MPPT under partial shading with fast dynamical change of hybrid load," *Sustainability*, vol. 14, no. 5, pp. 2937–2954, 2022.

[22] V. F. Pires, A. Cordeiro, D. Foito, and J. F. Silva, "Control transition mode from voltage control to MPPT for PV generators in isolated DC microgrids," *International Journal of Electrical Power & Energy Systems*, vol. 137, pp. 107876–107889, 2022.

[23] G. A. Raiker, U. Loganathan, and S. B. Reddy, "Current control of boost converter for PV interface with momentum-based perturb and observe MPPT," *IEEE Transactions on Industry Applications*, vol. 57, no. 4, pp. 4071–4079, 2021.

[24] K. Kumar, R. Tiwari, P. V. Varaprasad, C. Babu, and K. J. Reddy, "Performance evaluation of fuel cell fed electric vehicle system with reconfigured quadratic boost converter," *International Journal of Hydrogen Energy*, vol. 46, no. 11, pp. 8167–8178, 2021.

[25] A. K. Podder, N. K. Roy, and H. R. Pota, "MPPT methods for solar PV systems: a critical review based on tracking nature," *IET Renewable Power Generation*, vol. 13, no. 10, pp. 1615–1632, 2019.

[26] D. F. Teshome, C. H. Lee, Y. W. Lin, and K. L. Lian, "A modified firefly algorithm for photovoltaic maximum power point tracking control under partial shading," *IEEE Journal of Emerging and Selected Topics in Power Electronics*, vol. 5, no. 2, pp. 661–671, 2016.

[27] G. S. Krishnan, S. Kinattingal, S. P. Simon, and P. S. R. Nayak, "MPPT in PV systems using ant colony optimisation with dwindling population," *IET Renewable Power Generation*, vol. 14, no. 7, pp. 1105–1112, 2020.

[28] S. Titri, C. Larbes, K. Y. Toumi, and K. Benatchba, "A new MPPT controller based on the ant colony optimization algorithm for photovoltaic systems under partial shading conditions," *Applied Soft Computing*, vol. 58, pp. 465–479, 2017.

[29] M. Seyedmahmoudian, B. Horan, T. K. Soon et al., "State of the art artificial intelligence-based MPPT techniques for mitigating partial shading effects on PV systems - a review," *Renewable & Sustainable Energy Reviews*, vol. 64, pp. 435–455, 2016.

[30] Y. P. Huang, X. Chen, and C. E. Ye, "A hybrid maximum power point tracking approach for photovoltaic systems under partial shading conditions using a modified genetic algorithm and the firefly algorithm," *International Journal of Photoenergy*, vol. 2018, Article ID 7598653, 13 pages, 2018.

[31] B. Babes, A. Boutaghane, and N. Hamouda, "A novel nature-inspired maximum power point tracking (MPPT) controller based on ACO-ANN algorithm for photovoltaic (PV) system fed arc welding machines," *Neural Computing & Applications*, vol. 34, no. 1, pp. 299–317, 2022.

[32] H. Hamdi, C. B. Regaya, and A. Zaafouri, "Real-time study of a photovoltaic system with boost converter using the PSO-RBF neural network algorithms in a MyRio controller," *Solar Energy*, vol. 183, pp. 1–16, 2019.